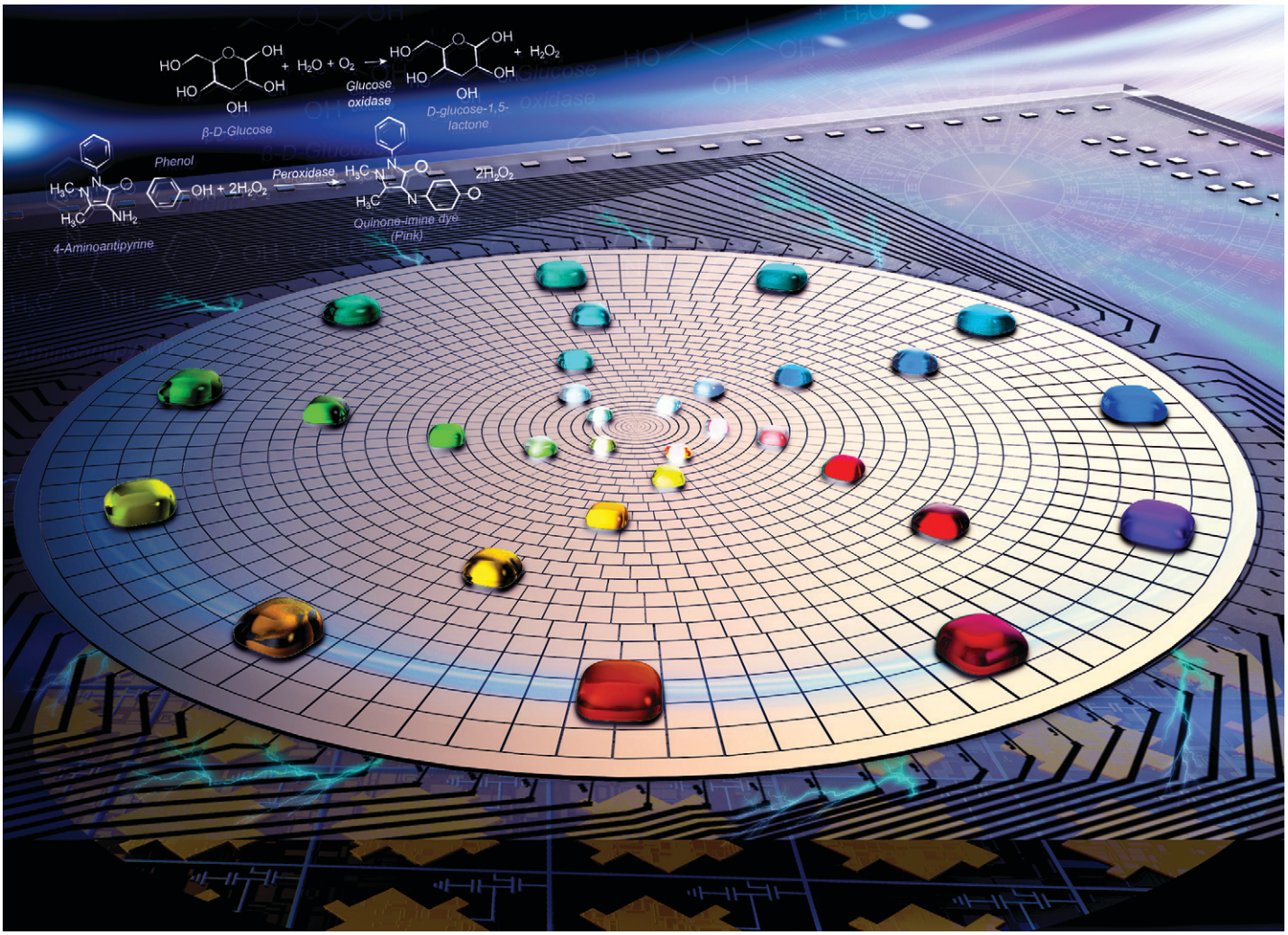

Featuring work from laboratories of Professor Hanbin Ma at Suzhou Institute of Biomedical Engineering and Technology, China, and Professor Jinhua Li at Changchun University of Science and Technology, China, and Guangdong ACXEL Micro & Nano Tech Co., Ltd, China, and ACX instruments Ltd, Cambridge, UK. ACXEL is a leading company that provides a one-stop solution for next-generation digital microfluidics system to fit into a wide range of application areas.

Polar coordinate active-matrix digital microfluidics for high-resolution concentration gradient generation

Automated concentration gradient generation is one of the most important applications of lab-on-a-chip devices. In this work, we report an active-matrix digital microfluidic device with polar coordinate electrodes arrangement. To compare with conventional rectangular coordinator arrangement with the similar electrode number, this work shows approximately a 19 times resolution enhancement for the achievable concentration gradient.

As featured in:

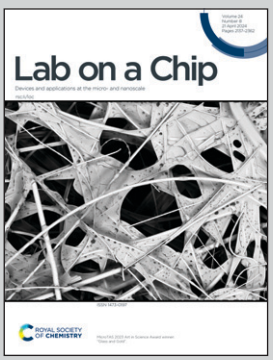

See Jinhua Li, Hanbin Ma *et al.*, *Lab Chip*, 2024, **24**, 2193.

ROYAL SOCIETY OF CHEMISTRY

rsc.li/loc

Registered charity number: 207890

Lab on a Chip

PAPER

View Article Online
View Journal | View Issue

Cite this: *Lab Chip*, 2024, **24**, 2193

Polar coordinate active-matrix digital microfluidics for high-resolution concentration gradient generation†

Bingbing Zhang, [ab] Jinxin Fu,[bc] Maohua Du,[d] Kai Jin,[b] Qi Huang,[b] Jiahao Li,[e] Dongping Wang, [b] Siyi Hu, [bd] Jinhua Li*[a] and Hanbin Ma *[bd]

Automated concentration gradient generation is one of the most important applications of lab-on-a-chip devices. Digital microfluidics is a unique platform that can effectively achieve digitalized gradient concentration preparation. However, the dynamic range and concentration resolution of the prepared samples heavily rely on the size and the number of effective electrodes. In this work, we report an active-matrix digital microfluidic device with polar coordinate electrode arrangement. The device contains 33 different electrode sizes, generating digital droplets of different volumes. To compare with the conventional rectangular coordinate arrangement with a similar electrode number, this work shows an approximately 19 times resolution enhancement for the achievable concentration gradient. We characterized the stability and uniformity of droplets generated by electrodes of different sizes, and the coefficient of variation of stable droplets was less than 3%. The fluorescent nanomaterial's concentration quantification and glucose concentration characterization experiments were also conducted, and the correlation coefficients for the linearities were all above 0.99.

Received 13th November 2023,
Accepted 23rd February 2024

DOI: 10.1039/d3lc00979c

rsc.li/loc

1 Introduction

In biochemical analysis, preparing samples with various concentration gradients is crucial for the systematic study of the interactions between samples and components of different concentrations.[1–3] The study of mechanisms and processes such as DNA analysis,[4] drug screening,[5,6] and immune analysis[7,8] all involves the analysis of concentration gradients of diffusible chemicals. However, traditional sample concentration gradient experiments are mainly conducted with assay plates, which not only require tedious and repetitive manual or mechanical operational steps, but also cannot guarantee accuracy and repeatability.[9]

Concentration gradient generators based on microfluidic chips have been rapidly developed in recent decades,[10–14] attracting significant attention due to their advantages such as low reagent consumption, ease of control, and automation.[15] Compared with macro-scale systems, the micro-scale characteristics of microfluidic devices can effectively reduce the use of chemical reagents and precious drugs.[16–18] However, traditional microfluidic chips require the construction of microchannels, micropump valves, or microwells on the chip, which limits the concentration gradient dilution method based on microfluidic technology to complex chip structures and devices, resulting in low operational flexibility and accuracy, limited integration and scalability, and limited application scenarios.

Electrowetting-on-dielectric (EWOD)[19–25] digital microfluidics (DMF) does not rely on microchannels or microstructures. It can achieve the construction of droplet manipulation systems such as movement, generation, splitting, and mixing under electrical signals.[26] Compared to conventional microfluidic technology, it can achieve more flexible control of digital droplets. Hsu[27] designed electrodes with different sizes and Kim[28] combined an EWOD device with real-time feedback control. Both have obtained droplets of different volumes and mixed sample reagents with different volume ratios successfully. These passive-matrix (PM) designs have relatively fewer electrodes, and consequently the layout design can be very flexible.

[a] *Nanophotonics and Biophotonics Key Laboratory of Jilin Province, Changchun University of Science and Technology, Changchun, 130022, P. R. China. E-mail: lijh@cust.edu.cn*
[b] *CAS Key Laboratory of Bio-medical Diagnostics, Suzhou Institute of Biomedical Engineering and Technology, Chinese Academy of Sciences, No. 88 Keling Road, Suzhou, Jiangsu Province, 215163, P. R. China. E-mail: mahb@sibet.ac.cn*
[c] *School of Biomedical Engineering (Suzhou), Division of Life Sciences and Medicine, University of Science and Technology of China, Hefei 230027, Anhui, P. R. China*
[d] *Guangdong ACXEL Micro & Nano Tech Co., Ltd, Guangdong Province, 528000, P. R. China*
[e] *ACX Instruments Ltd, St John's Innovation Centre, Cowley Road, Cambridge, CB4 0WS, UK*

† Electronic supplementary information (ESI) available. See DOI: https://doi.org/10.1039/d3lc00979c

However, the preparation of concentration gradient samples by DMF heavily relies on the number of effective electrodes on the chip. Active-matrix (AM) EWOD with thin-film electronics can effectively increase the number and density of electrodes, allowing it to manipulate more droplets[29,30] and achieve higher concentration resolutions. The resolution here is defined as the difference between two adjacent achievable generated concentrations. This technology integrates thin film electronics in pixels as a switching element, and more layers of thin-film materials with complexed design rules need to be followed.

Li[31] reported EWOD technology compatible with CMOSs, and Rack[32] extended it to be compatible with thin film transistors (TFTs). Morgan[33] designed a 64 × 64 array AM-EWOD device with impedance sensor functionality. Ma[22,30] utilized a Si TFT to manufacture an AM-EWOD device and designed hexagonal electrodes. To the best of our knowledge, to date, all existing reported AM-EWOD devices are designed in rectangular coordinates with rectangular-shaped electrodes. In EWOD, the generated droplet volume is determined by the size of the electrodes. With a rectangular electrode arrangement, the droplet volume can only be an integer multiple of the minimum electrode control unit. Therefore, the difference in the mixing ratio is limited by the minimum unit, which restricts the accuracy of concentration gradient and resolution.

In this work, we creatively designed an AM-EWOD device in polar coordinates. The electrodes are distributed in 33 concentric circles, where the electrode size changes gradually in different circles. This allows a smooth change in controlled droplet volume from 0.03 nL to 3.29 nL. The volume of the smallest droplet is only 0.9% of the volume of the largest droplet, and each droplet can be addressed and moved to a designated area. This design overcomes the 'integer multiple' droplet volume limitation in conventional rectangular AM-EWOD devices and enhances the sample concentration resolution by a factor of 19 times in concentration gradient generation applications.

2 Experimental

2.1 Reagents and materials

Silicone oil (2 cSt) was purchased from Dow Corning Corporate. Carbon quantum dots (CQDs) solution was purchased from Suzhou Xingshuo Nanotechnology Co., Ltd. (China), with a concentration of 10 mg mL^{-1}, an excitation wavelength of 480 nm, and a photoluminescence wavelength of 514 nm. Phosphate buffered saline (PBS) was procured from Shenggong Biotechnology (Shanghai, China) Co., Ltd., while edible pigments were sourced from Shanghai Fengwei Industrial Co., Ltd (China). Glucose powder was procured from China National Pharmaceutical Group Chemical Reagent Co., Ltd (China). And a glucose content detection kit was obtained from Beijing Solarbio Science & Technology Co., Ltd (China).

The ATP1010 miniature spectrometer used in this study was acquired from Optosky Optical (Xiamen, China). Customised fibre UV200-FC, featuring a core diameter of 200 μm, a length of 0.4 m, and a NA value of 0.22, was acquired from Xiamen Jitan Technology (China). This fibre was equipped with a SMA905+FC interface and UV5-10 fibre collimating convergence lens, which were all purchased from Xiamen Jitan Technology (China). The experimental setup was powered by a DP832A power supply used in this study, a product of RIGOL Technologies (China). The NIKON microscope was model NI-U, and the camera model MV-CS050-10GC was from Hikvision (China).

2.2 Chip design and manufacturing

The AM-EWOD chip was manufactured using the standard flat panel display process of TIANMA Microelectronics (Shenzhen, China), comprising an a-Si thin film transistor (TFT)[32] electrode array on a 0.5 mm thick glass substrate, an electrowetting dielectric layer of 300 nm Si_3N_4, and a spin-coated hydrophobic layer of 100 nm, a top ITO glass plate with sample loading holes, and a UV adhesive mixed with standard-sized glass microspheres (20 μm) for gap control and packaging. For information on gap dimensions, please refer to ESI† Fig. S1. The chip assembly was carried out by ACXEL Micro&Nano Tech (Foshan, China). As shown in Fig. 1(a and b), our electrode arrangement was designed based on polar coordinates. However, due to the limitations of lithography technology wiring, continuous angle transformation was not feasible. Consequently, we segmented the arrangement according to the minimum line width, resulting in the creation of 33 electrode areas. For more detailed information, please refer to ESI† Table S1. Each pixel electrode, as shown in Fig. 1(c), includes a TFT and a capacitor, forming a 1T1C circuit. Due to limitations in the TFT process design, unlike the pixel circuit of 7–32 laps, the 0–6 laps use a 1T0C circuit. ESI† Fig. S2 illustrates the AM-EWOD chip, driven by TFT, which requires two types of signals: source-addressed V_{data} and gate-addressed V_{gate}. In this work, the V_{data} line was aligned along a concentric circle, while the V_{gate} line was oriented perpendicular to the V_{data} line. As the electrodes are arranged in a polar coordinate system, the shape of each electrode resembles that of a fan ring. A layer of polytetrafluoroethylene (from Chemours) was applied on the surface of the top and bottom plates as a hydrophobic layer. Finally, adhesive was applied along the edge of the top plate, after which the bottom plate was firmly pressed and sealed. The space between the two boards was filled with silicone oil, acting as a medium for the movement of reagents. The conductive ITO was connected to the system ground using silver paste, and a custom-designed flexible printed circuit (FPC) was attached to the chip. Fig. 1(a) illustrates the complete view of the AM-EWOD chip. Fig. 1(d) shows the design sketch and parameter information of the AM-EWOD chip and traditional rectangular coordinate chip. Both of them have the same effective on-chip area and a similar number of electrodes. In this study, comparative experiments will be

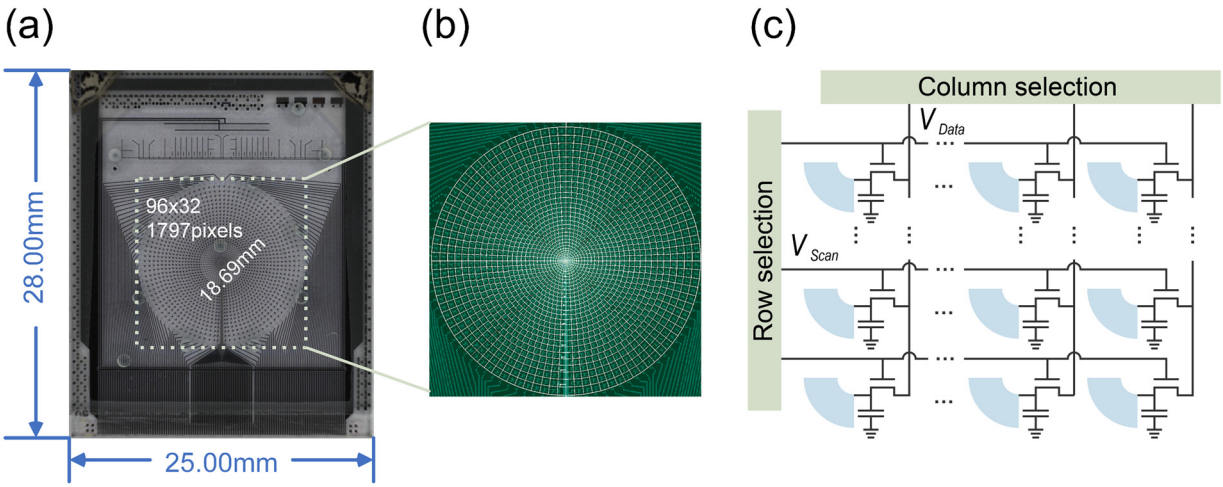

(d)

Two designs	Polar coordinate design with multiple types of electrodes	Rectangular coordinate design with a single type of electrode
	1.32*10⁴ um; 96 x 32; 1797 pixels	1.17*10⁴ um; 43 x 43; 1849 pixels
Array Size (um²)	1.37*10⁸	1.37*10⁸
Pixel Size (um)	32.9-405	272
Droplet Gap (um)	20	20
Ideal Droplet Volume (nL)	0.03-3.29	1.48
Actual Droplet Volume (nL)	0.45-3.29	1.48

Fig. 1 AM-EWOD chip for high-resolution concentration gradient generation. (a) A photograph of the AM-EWOD chip. (b) Polar coordinate electrode layout. (c) Pixel circuit schematics. (d) Parameter diagram of two types of chip designs.

conducted based on this standard. The AM-EWOD chip has a wider size range and smaller electrode, and consequently it can produce a wider volume range and smaller droplets than traditional designs. Therefore, under the same comparison criteria, the concentration resolution between the two designs will be different.

2.3 Fluorescence detection system design

The prototype of the DMF fluorescence detection system is shown in ESI† Fig. S3, consisting of a DMF droplet control module, a detection module, and a two-axis control module. The droplet control module can independently control 1797 electrodes. Custom-designed control software was developed for droplet manipulations, featuring a robust pre-editing capability for defining droplet motion paths. In this setup, an AM-EWOD chip was connected to the control board. The two-axis control system offers positioning, timing, and arbitrary control functions to provide the mosaic imaging of the entire chip. For the fluorescence detection module, we used a miniature fluorescence module purchased from Suzhou MoNeSi Optoelectronic Technology Co., Ltd. To achieve the desired light spot size, we employed a 20× objective lens and aligned it with a two-axis system, placed vertically above the chip. In this experiment, 480 nm light was utilized to excite different concentrations of CQDs, while the optical detection module captured and recorded changes in fluorescence intensity.

2.4 Absorbance detection system design

The prototype of the DMF absorbance detection system is shown in ESI† Fig. S4. It comprises a fibre optic spectrometer as the detection end, connected to a collimating lens *via* a custom 0.4 m fibre optic cable. The probe was secured above the AM-EWOD chip *via* a customized clip, and the light source structure below the chip features a 0.4 mm circular aperture, that is coaxial with the centre of the lens above the chip. During the reaction process of the test sample, parallel light passed through the chip and the test sample within it. The optical detection module collected and recorded the changes in the optical signal. In this experiment, a 505 nm LED light source was used to detect the linear curves of glucose reactions at different concentrations on the chip.

3 Results and discussion

3.1 Droplet uniformity and stability analysis

As a fully automated micro/nano fluid precision processing system, the storage tank of the digital microfluidic chip undertakes the function of sample and reagent injection. The uniformity and stability of droplets are crucial factors that determine the effectiveness and reliability of the AM-EWOD chip. The relative volume deviation of droplet distribution directly affects the efficiency and yield of the reaction. If the distance between the upper and lower plates of the fixed chip is fixed, the volume of the droplet is only determined by its top view area. A DI droplet is introduced into the storage tank, droplets are continuously generated through the tank, and an upright microscope is used to capture real-time images of the droplets.

The droplet contour is captured through image analysis software ImageJ and fine processing and analysis are performed, the top view area of the droplets is measured, and then the volume of each droplet is calculated based on the known distance between the two plates. Fig. 2(a) and Video S1† show the percentage of droplet generation for different sizes. Due to the use of a 1T0C circuit for 0–6 laps, the lack of capacitance makes it difficult to maintain a stable driving voltage, resulting in the inability of 0–6 laps to generate droplets. The success rates of generating droplets for the 7th, 8th and 9th laps are 10%, 60% and 70%. The success rate of generating droplets from the 10th to 32nd laps is 100%. The limitation of generating the smallest droplet on AM-EWOD chips is related to the gap and droplet size ratio. When the generation approaches the limit of droplet size, the value of CV will also deteriorate. Fig. 2b and Video S1† show the footprint of droplets of different sizes, and the overall trend is consistent with the actuated pixel area. Please refer to ESI† Fig. S5. Fig. 2c shows the uniformity of droplets from the 8th to the 32nd laps, with a CV of less than 3% for droplets from the 10th to the 32nd laps.

3.2 Efficiency and resolution

The fewer times a droplet is manipulated, the more efficient it is. For example, when preparing a certain concentration, the required volume ratio for the two reagents should be determined. On the conventional AM-EWOD chip with a rectangular coordinate electrode arrangement, the number of times a droplet is manipulated can be calculated by the total product of the required reagent divided by the volume of a single-pixel droplet, resulting in low operational flexibility. But on the AM-EWOD chip with a polar coordinate electrode arrangement, complex operations can be avoided. In the presence of multiple electrodes, the simplest method is the greedy algorithm, which prioritizes selecting larger droplets and then sequentially approaches the target volume with smaller droplets. As shown in Fig. 3(d), the operational complexity of the rectangular coordinate design with a single type of electrode increases linearly. Compared to this, the polar coordinate design can easily mix the desired volume ratio, and as the volume demand increases, the absolute advantage becomes more apparent. Therefore, the polar coordinate design is much more efficient in completing concentration sample preparation.

As shown in Fig. 3(e) and Videos S2 and S3,† we take two reagents mixed in a 3 : 10 ratio as an example. In the case of

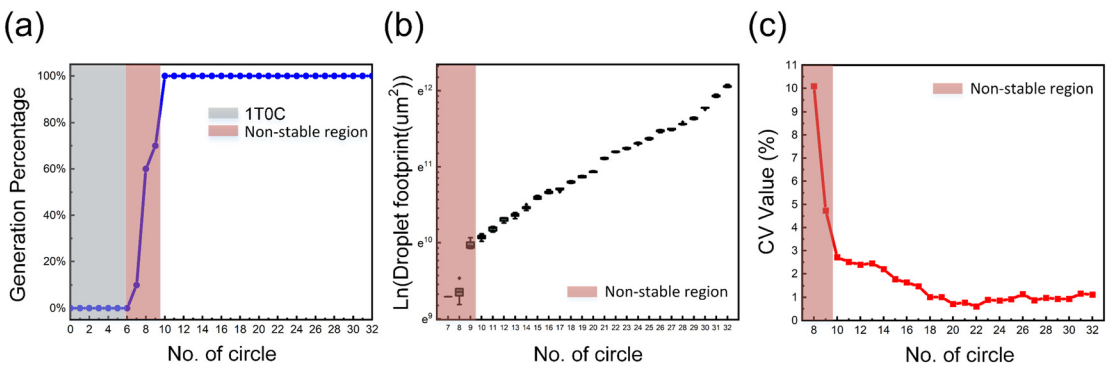

Fig. 2 Characterization data of uniformity and stability: (a) the success rate of producing droplets of different sizes. (b) The footprint of droplets produced by pixels of different sizes. (c) The CV value of the volume of droplets produced by different pixels.

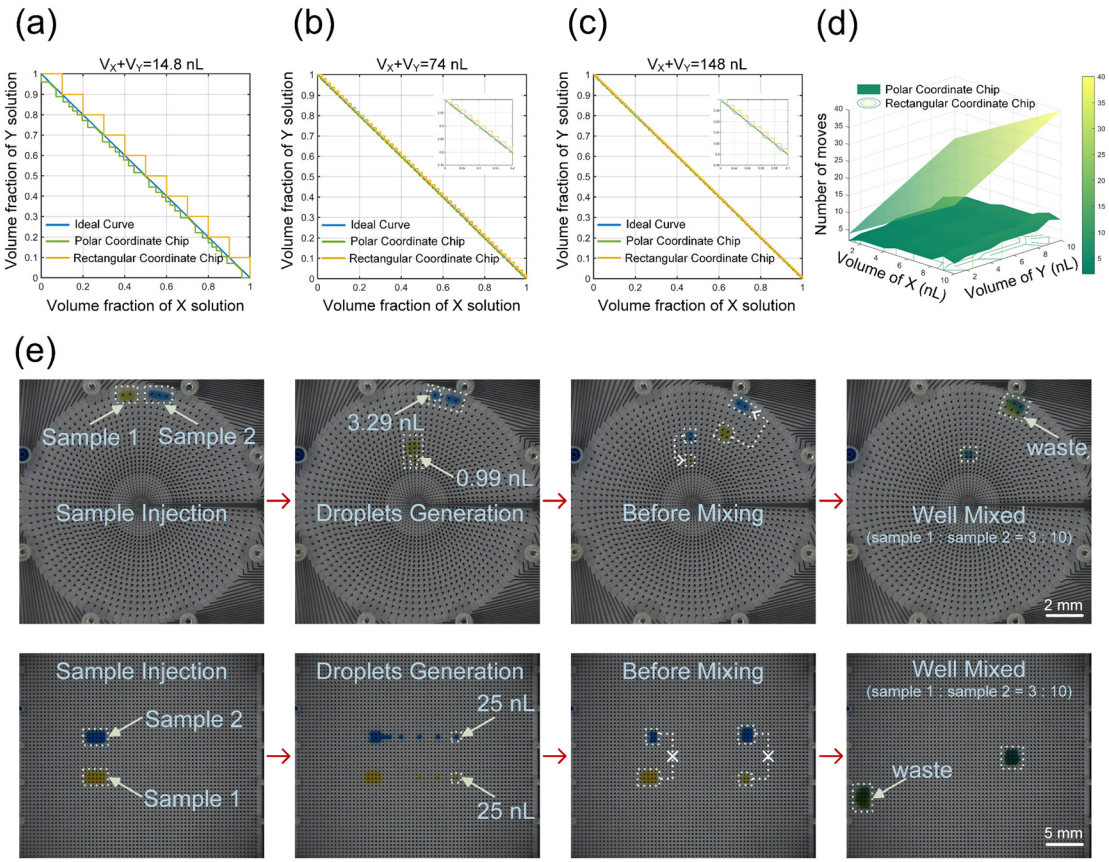

Fig. 3 Comparison of two kinds of electrode designs on the chip: (a–c) comparison of the concentration resolution of two chip designs at a total sample size (V_X + V_Y) of 14.8 nL, 74 nL, and 148 nL. (d) Comparison of the complexity of preparing solutions using the polar coordinate chip with multiple electrodes and the rectangular coordinate chip with a single type of electrode. (e) Efficiency differences between the two chip designs when mixing two reagents at a 3 : 10 ratio described through screenshots from Videos S2 and S3† at four different time points.

using the same tearing method, the rectangular coordinate design requires 13 steps to complete the entire mixing process, while the polar coordinate design only needs to find the corresponding volume ratio of two droplets, such as 0.99 nL in the 19th lap and 3.29 nL in the 32nd lap, to directly complete the 3 : 10 ratio mixing through two steps, which reflects the higher efficiency of the polar coordinate design in the configuration more intuitively.

In biological applications, the accuracy of concentration is important. The resolution of solution dilution is related to the total sample volume and the minimum volume achievable by the droplet. As shown in Fig. 1(d), we believe that comparing the concentration resolution based on this benchmark is fair. The dilution ratio of both designs is V_X : V_Y, where the AM-EWOD chip can stably produce a minimum droplet volume of 0.45 nL, while the traditional rectangular coordinate chip with a single type of electrode can produce a minimum droplet volume of 1.48 nL. Fig. 3(a) shows the concentration resolution of both at V_X + V_Y = 14.8 nL. Within the concentration range of 0–1, the AM-EWOD chip can produce 207 gradient concentrations using the greedy algorithm, while traditional methods can only produce 10 gradient concentrations. The specific configuration plan is provided in the ESI† (Excel). Fig. 3(b) and (c) illustrate the concentration resolution at V_X + V_Y = 74 nL and 148 nL. The AM-EWOD chip can generate 977 and 1978 gradient concentrations, respectively, while the traditional rectangular coordinate can only generate 50 and 100 gradient concentrations, separately. The subgraph shows the concentration of both within a small range. The results indicate that as the total sample volume increases, both designs can generate more concentrations, but AM-EWOD chips always achieve higher concentration resolution.

3.3 Fluorescence concentration gradient generation experiments

Fluorescence imaging plays an important role in biomedicine, as it can be used to label molecules such as cells, proteins, and DNA for research in cell imaging, drug screening, and other fields. Therefore, we use fluorescence gradients to characterize the ability of polar coordinate systems to generate concentration gradients.

Firstly, 1× PBS was added to a 10 mg ml^{-1} CQDs solution for dilution to prepare a 2.5 mg ml^{-1} CQDs solution, which we define as the concentration of 2×. As shown in Fig. 4(a) and Video S4,† a 2× CQDs solution was injected into the chip, and the droplets split, mixed, and moved in a pre-

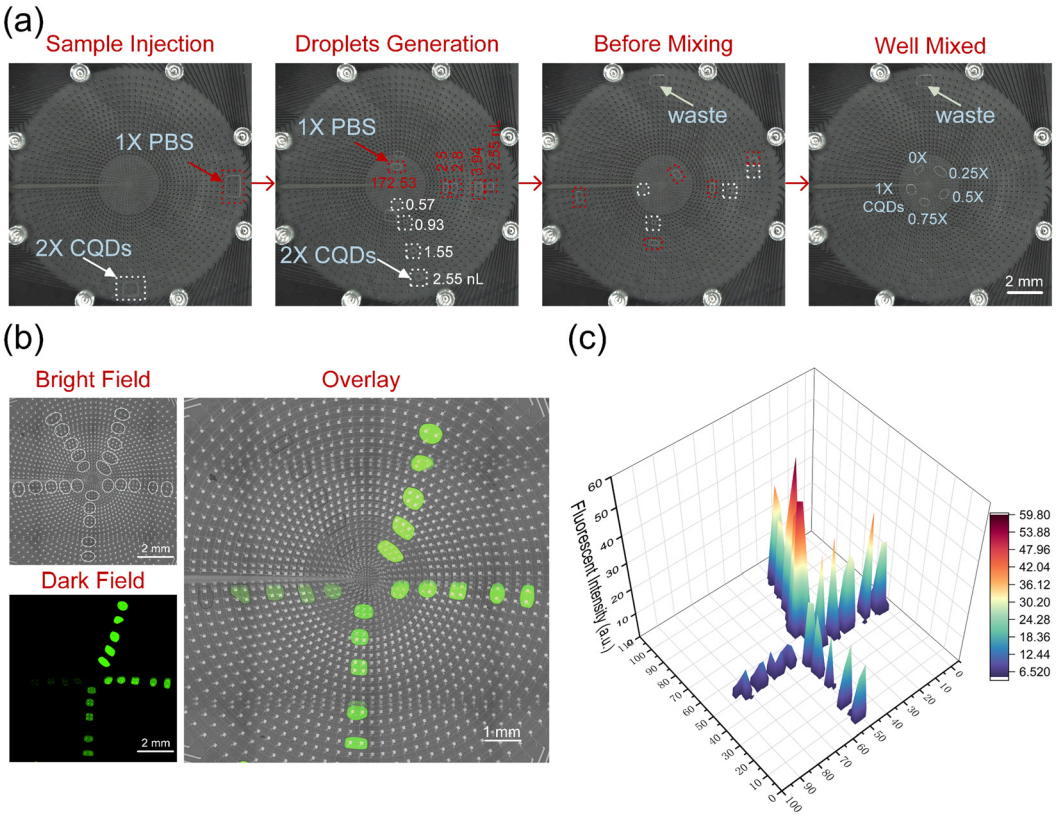

Fig. 4 Gradient of droplet fluorescence: (a) four screenshots from Video S4† illustrate the mixing of deionized water and CQDs solution with different volumes on the AM-EWOD chip. (b) Bright-field, dark-field, and overlay images of fluorescent solutions with varying concentrations. (c) 3D stereogram of fluorescence for solutions with different concentrations.

programmed program. The gradients of 0×, 0.25×, 0.5×, 0.75×, and 1× were mixed on the chip using PBS, and the experiment was repeated 5 times to form a gradient fluorescent droplet array. As shown in Fig. 4(b), the bright field and dark field images of five parallel gradient CQDs solutions with different concentrations are displayed, clearly reflecting that the higher the concentration of the sample, the brighter the fluorescence microscopy image. As shown in Fig. 4(c), the fluorescence intensity values of different droplets were also extracted, and the trend of the fluorescence intensity values was consistent with the trend presented in the fluorescence microscopy image. The stability and repeatability of the experimental results were demonstrated through 5 parallel sets of 20 droplets, and the AM-EWOD chip can efficiently achieve high-throughput and high-resolution concentration sample preparation.

The above experiment indicates that concentration gradient dilution of CQDs can be achieved on an AM-EWOD chip, but the above system has not been quantitatively analysed. To achieve quantitative analysis of CQDs, we have built a computer-controlled biaxial system to perform full scan detection of CQDs on the chip. The optical detection device is shown in ESI† Fig. S3. To maximize the utilization of chip area, we also mixed gradients of 0×, 0.25×, 0.5×, 0.75×, 1×, 1.25×, 1.5×, 1.75×, and 2× on the chip using the same method.

As shown in Fig. 5(a), the bright field, dark field, and overlay images of CQDs solutions with different concentrations are displayed. As shown in Fig. 5(b), a full scan was performed on the chip with 9 samples at a step size of 500 μm. To exclude the influence of dark backgrounds, the fluorescence values of the locations without a sample and with the 0× sample were deducted, and the fluorescence intensity of the remaining samples increased with increasing concentration. As shown in Fig. 5(c), the fluorescence intensity is consistent with the trend of the thermal map. As shown in Fig. 5(d), the fluorescence intensity of CQDs increases with increasing concentration. The correlation coefficient of the corresponding linear fitting curve is 0.9941. The experimental results show that the system can reproduce the results of fluorescence microscopy and perform fluorescence quantitative analysis on samples.

3.4 Glucose concentration experiments

Glucose is one of the main substances in the human energy metabolism. Glucose detection can determine whether there is abnormal blood sugar in the human body, and it is often used in the diagnosis and treatment of diabetes. Under normal circumstances, the glucose content of a normal person's sample on an empty stomach in the morning is 80–120 mg dl^{-1}.[34] As shown in Fig. 6(b), the principle of the

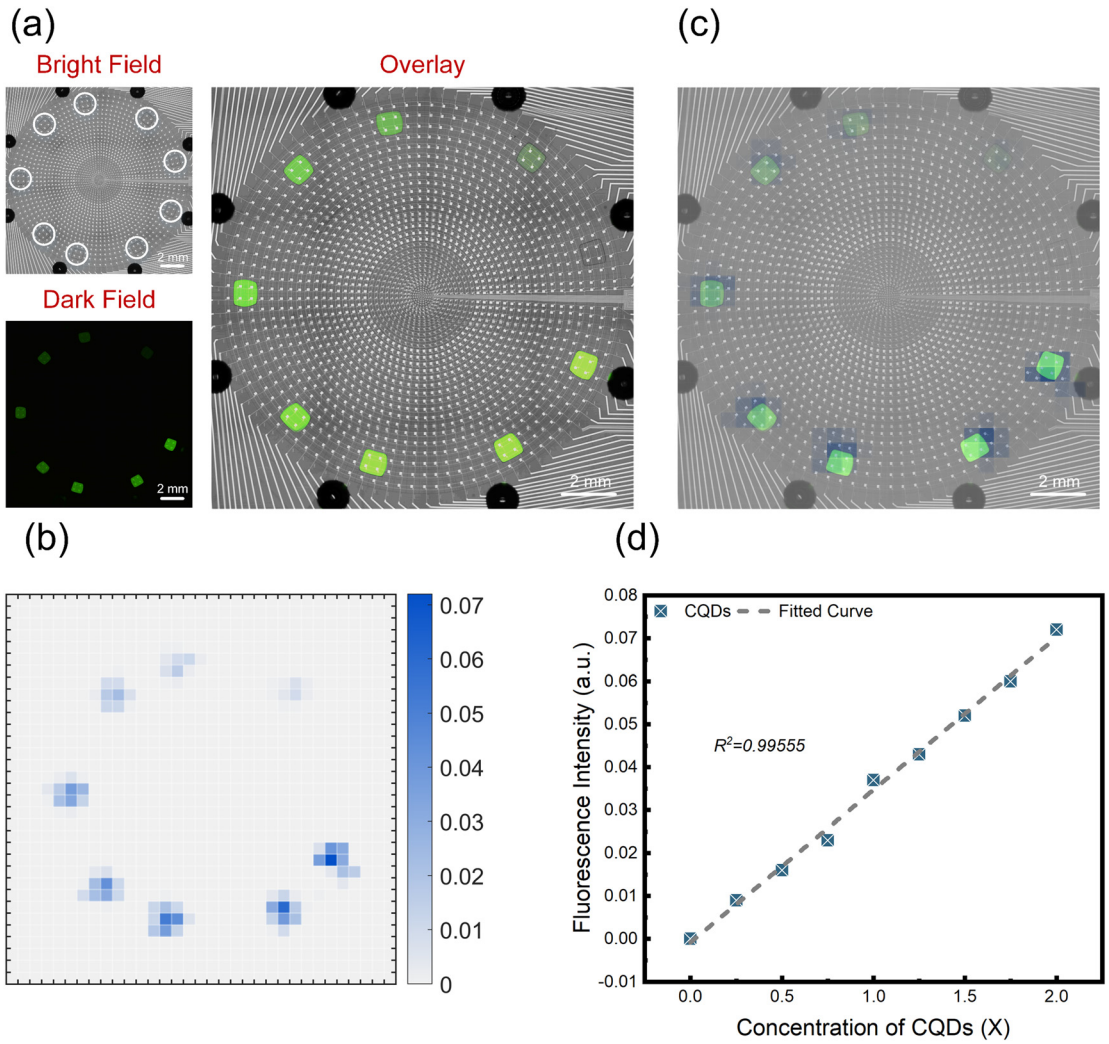

Fig. 5 Quantitative fluorescence analysis experiments: (a) bright-field, dark-field, and overlay images of fluorescent solutions with varying concentrations. (b) Heatmap of fluorescent solutions with different concentrations. (c) Overlay images of bright-field, dark-field, and heatmap for solutions with different concentrations. (d) Graph depicting the relationship between fluorescence intensity and concentration of fluorescent solutions.

glucose determination reaction is shown. Glucose is oxidized by glucose oxidase to produce gluconic acid and hydrogen peroxide, and then coupled with the oxidase to oxidize colourless 4-aminoantipyridine and condense phenol to form red quinone imine. This substance has a maximum absorption peak at 505 nm, and its absorbance is proportional to the glucose content. As shown in Fig. 6(a) and Video S5,† we mixed 5 glucose detection solutions with different concentrations of 72, 100, 132, 164, and 200 mg dl^{-1} on the chip and reacted them at 25 °C for 15 minutes. The experimental concentration is very close to the warning value of blood sugar, which can provide more accurate monitoring of the human blood sugar status. As shown in Fig. 6(c), the standard curve obtained by analysing glucose detection solutions with known concentrations on the testing platform is shown. The dynamic range of the standard curve covers the normal blood glucose range of the human body, and the error bar represents the standard deviation between three measurements. The correlation coefficient (R^2) of the standard curve is 0.99045. The results indicate that the DMF system can process glucose samples and detect them.

Conclusions

In this paper, we present a novel AM-EWOD chip with a polar coordinate electrode arrangement, featuring electrodes arranged on concentric circles of varying diameters. This unique design enables the DMF chip to efficiently generate high-resolution concentration gradients, surpassing the limitations of the conventional rectangular coordinate layout. This pioneering technology significantly expands the capabilities of digital microfluidics, representing a key step towards realising a comprehensive 'lab-on-a-chip' platform.

Author contributions

B. Z., M. D. and H. M. conceived the design. B. Z., J. L. and S. H. designed the experiments. B. Z. and J. F. performed the

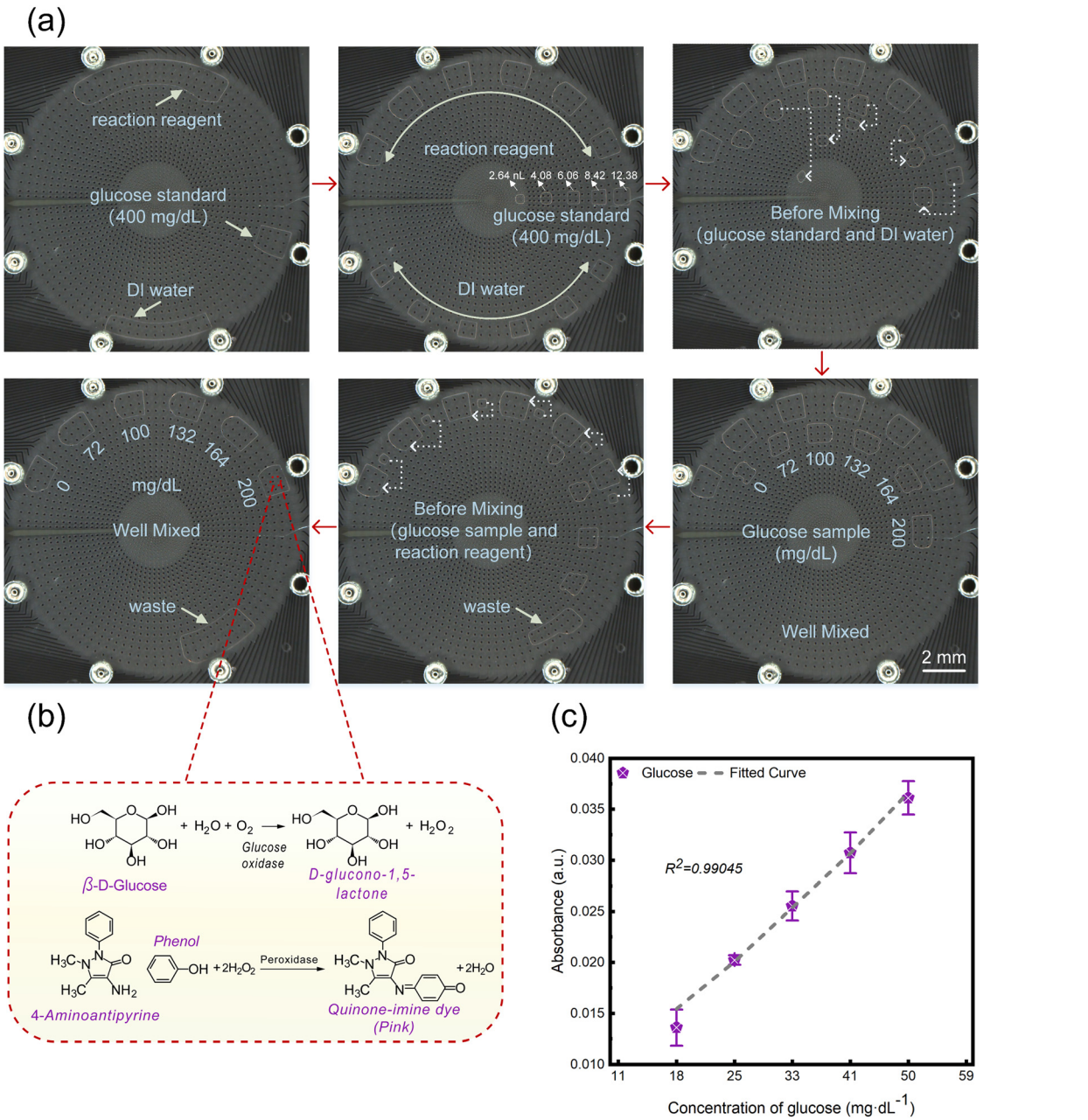

Fig. 6 Glucose concentration experiments: (a) screenshot pictures of the glucose reaction workflow. (b) Schematic illustration of the principle of the glucose reaction. (c). Graph illustrating the relationship between different concentrations of glucose solution and absorbance.

experiments and wrote the manuscript. K. J., Q. H., J. L. and D. W. offered professional advice for the manuscript. All authors reviewed and commented on the manuscript.

Conflicts of interest

There are no conflicts to declare.

Acknowledgements

This work was supported by the National Key R&D Program of China (2023YFF0721500), the National Natural Science Foundation of China (No. 62374102), the Jilin Scientific and Technical Development Program (20210204110YY), the China Postdoctoral Science Foundation (2022M722338), the Science and Technology Innovation Project of Foshan, Guangdong Province, China (1920001000047), the Innovation and Entrepreneurship Team Project of Jiangsu Province (JSSCTD202145), and the Project of Education Department of Jilin Province (JJKH20230794KJ).

Notes and references

1 B. L. Khoo, G. Grenci, Y. B. Lim, S. C. Lee, J. Han and C. T. Lim, *Nat. Protoc.*, 2018, **13**, 34–58.

2 B. Nguyen, P. J. Graham, C. M. Rochman and D. Sinton, *Adv. Sci.*, 2018, **5**, 1700677.
3 S. Hu, Y. Jie, K. Jin, Y. Zhang, T. Guo, Q. Huang, Q. Mei, F. Ma and H. Ma, *Biosensors*, 2022, **12**, 324.
4 Y.-H. Chang, G.-B. Lee, F.-C. Huang, Y.-Y. Chen and J.-L. Lin, *Biomed. Microdevices*, 2006, **8**, 215–225.
5 L. Yin, G. Du, B. Zhang, H. Zhang, R. Yin, W. Zhang and S.-M. Yang, *Sci. Rep.*, 2020, **10**, 6568.
6 Y. Luo, X. Zhang, Y. Li, J. Deng, X. Li, Y. Qu, Y. Lu, T. Liu, Z. Gao and B. Lin, *RSC Adv.*, 2018, **8**, 25409–25416.
7 A. H. C. Ng, R. Fobel, C. Fobel, J. Lamanna, D. G. Rackus, A. Summers, C. Dixon, M. D. M. Dryden, C. Lam, M. Ho, N. S. Mufti, V. Lee, M. A. M. Asri, E. A. Sykes, M. D. Chamberlain, R. Joseph, M. Ope, H. M. Scobie, A. Knipes, P. A. Rota, N. Marano, P. M. Chege, M. Njuguna, R. Nzunza, N. Kisangau, J. Kiogora, M. Karuingi, J. W. Burton, P. Borus, E. Lam and A. R. Wheeler, *Sci. Transl. Med.*, 2018, **10**, eaar6076.
8 K. Jin, C. Hu, S. Hu, C. Hu, J. Li and H. Ma, *Lab Chip*, 2021, **21**, 2892–2900.
9 ISO, *ISO 8655-2 Piston-operated volumetric apparatus — Part 2: Pipettes*, Switzerland, 2022.
10 H. Song, D. L. Chen and R. F. Ismagilov, *Angew. Chem., Int. Ed.*, 2006, **45**, 7336–7356.
11 S.-Y. Teh, R. Lin, L.-H. Hung and A. P. Lee, *Lab Chip*, 2008, **8**, 198–220.
12 D. T. Chiu, R. M. Lorenz and G. D. M. Jeffries, *Anal. Chem.*, 2009, **81**, 5111–5118.
13 A. B. Theberge, F. Courtois, Y. Schaerli, M. Fischlechner, C. Abell, F. Hollfelder and W. T. S. Huck, *Angew. Chem., Int. Ed.*, 2010, **49**, 5846–5868.
14 R. R. Pompano, W. Liu, W. Du and R. F. Ismagilov, in *Annual Review of Analytical Chemistry, vol. 4*, ed. R. G. Cooks and E. S. Yeung, 2011, vol. 4, pp. 59–81.
15 J. Tan, S. Sun, D. Jiang, M. Xu, X. Chen, Y. Song and Z. L. Wang, *Mater. Today*, 2022, **58**, 201–220.
16 N. L. Jeon, S. K. W. Dertinger, D. T. Chiu, I. S. Choi, A. D. Stroock and G. M. Whitesides, *Langmuir*, 2000, **16**, 8311–8316.
17 C. Samson and A. Koh, *Front. Bioeng. Biotechnol.*, 2020, **8**, 1037.
18 D. Rodin, M. Kirby, N. Sedogin, Y. Shapiro, A. Pinhasov and A. Kreinin, *Clin. Biochem.*, 2019, **65**, 15–20.
19 H. Ma, S. Hu, Y. Jie, K. Jin and Y. Su, *RSC Adv.*, 2020, **10**, 4899–4906.
20 M. G. Pollack, R. B. Fair and A. D. Shenderov, *Appl. Phys. Lett.*, 2000, **77**, 1725–1726.
21 K. Choi, A. H. C. Ng, R. Fobel and A. R. Wheeler, in *Annual Review of Analytical Chemistry, vol. 5*, ed. R. G. Cooks and E. S. Yeung, 2012, vol. 5, pp. 413–440.
22 H. Ma, S. Shi, K. Jin, D. Wang, S. Hu, Y. Su, Y. Zhang, J. Li, Z. Liu, C. Jiang, L. Feng, X. Guo and A. Nathan *Ieee, Electr. Network*, 2020.
23 B. Berge, *C. R. Acad. Sci., Ser. II: Mec., Phys., Chim., Sci. Terre Univers*, 1993, **317**, 157–163.
24 J. Lee, H. Moon, J. Fowler, T. Schoellhammer and C. J. Kim, *Sens. Actuators, A*, 2002, **95**, 259–268.
25 W. C. Nelson and C.-J. C. Kim, *J. Adhes. Sci. Technol.*, 2012, **26**, 1747–1771.
26 S. K. Cho, H. J. Moon and C. J. Kim, *J. Microelectromech. Syst.*, 2003, **12**, 70–80.
27 Y.-B. Wang, J.-H. Huang, M.-S. Lee, C.-Y. Huang, C.-S. Huang, I. Yamashita, Y.-Y. Tu and W. Hsu, *Microsyst. Technol.*, 2017, **23**, 3645–3651.
28 J. Gong and C.-J. Kim, *Lab Chip*, 2008, **8**, 898–906.
29 C. Hu, K. Jin and H. Ma, *Appl. Phys. Lett.*, 2023, **122**, 181601.
30 S. Hu, J. Ye, S. Shi, C. Yang, K. Jin, C. Hu, D. Wang and H. Ma, *Anal. Chem.*, 2023, **95**, 6905–6914.
31 Y. Li, W. Parkes, L. I. Haworth, A. A. Stokes, K. R. Muir, P. Li, A. J. Collin, N. G. Hutcheon, R. Henderson, B. Rae and A. J. Walton, *Solid-State Electron.*, 2008, **52**, 1382–1387.
32 J. H. Noh, J. Noh, E. Kreit, J. Heikenfeld and P. D. Rack, *Lab Chip*, 2012, **12**, 353–360.
33 B. Hadwen, G. R. Broder, D. Morganti, A. Jacobs, C. Brown, J. R. Hector, Y. Kubota and H. Morgan, *Lab Chip*, 2012, **12**, 3305–3313.
34 A. H. Mokdad, E. S. Ford, B. A. Bowman, D. E. Nelson, M. M. Engelgau, F. Vinicor and J. S. Marks, *Diabetes Care*, 2000, **23**, 1278–1283.